Chinese Journal of Physics 97 (2025) 933–947

Contents lists available at ScienceDirect

Chinese Journal of Physics

journal homepage: www.elsevier.com/locate/cjph

Research paper

On symmetry solutions of nonlocal complex coupled dispersionless system using Darboux transformation and artificial neural networks

Aamir Farooq [a], H.W.A. Riaz [b], Wen Xiu Ma [a,c,d,e,*]

[a] Department of Mathematics, Zhejiang Normal University, 321004, PR China
[b] Department of Physics, Zhejiang Normal University, 321004, PR China
[c] Department of Mathematics, King Abdulaziz University, Jeddah, 21589, Saudi Arabia
[d] Department of Mathematics and Statistics, University of South Florida, Tampa, FL 33620-5700, USA
[e] Material Science Innovation and Modelling, North-West University, Mafikeng Campus, Private Bag X2046, Mmabatho 2735, South Africa

ARTICLE INFO

Keywords:
Integrability
Soliton dynamics
Levenberg–Marquardt artificial neural network
Nonlinear wave interactions

ABSTRACT

The generalized coupled dispersionless equations describe the dynamics of a current-fed string in an external magnetic field. This study introduces a novel methodology leveraging the Darboux transformation to derive analytical solutions for these complex equations. The approach explores symmetry-preserving and non-preserving solutions, further refined using the Levenberg–Marquardt algorithm within a neural network framework. The network underwent thorough validation using relative L_2 errors during training and testing on clean and noisy data. During this validation, thorough tabular and graphical representations validated our analytical results, proving their reliability. We carefully analyzed the solution behaviors using various visualization techniques, such as contours, three-dimensional plots, and corresponding error graphs. This study comprehensively analyzes the system's dynamics by integrating analytical methods with artificial neural networks, bridging theoretical predictions with empirical validations. The findings offer new insights into wave behavior, stability, and nonlinear interactions within the system, contributing significantly to mathematical physics.

1. Introduction

Coupled dispersionless equations represent a system of nonlinear partial differential equations characterized by nonlinear interactions. These systems have garnered attention for their significance in various physical and engineering contexts, particularly in areas where wave dynamics play a crucial role. The generalized coupled dispersionless (CD) system describes the dynamics of a current-fed string in a specific external magnetic field, underscoring its relevance in practical applications [1]. These systems are suitable for modeling situations with limited dispersion effects, enabling researchers to focus on key non-linear interactions. Studying these equations deepens our understanding of wave structure formation, stability, and the potential for chaotic behavior under certain conditions, which aids in both theoretical advancements and practical applications.

The equations governing this system are given by

$$\rho_t + (rs)_x = 0, \quad r_{xt} - 2\rho r = 0, \quad s_{xt} - 2\rho s = 0,$$

where $\rho = \rho(x, t)$, $r = r(x, t)$, and $s = s(x, t)$ are scalar functions. By substituting $s = r$, the system reduces to the real CD system. Conversely, if we set $s = r^*$, we have a complex coupled dispersionless (CCD) system. These equations are called

* Corresponding author.
E-mail addresses: aamirf@zjnu.edu.cn (A. Farooq), wajahat@zjnu.edu.cn (H.W.A. Riaz), mawx@cas.usf.edu (W.X. Ma).

https://doi.org/10.1016/j.cjph.2025.07.021
Received 22 January 2025; Received in revised form 5 May 2025; Accepted 18 July 2025
Available online 29 July 2025

dispersionless because they do not include a dispersive term. Even without this term, they display intricate behaviors such as periodic solutions, rational solutions, bright and dark soliton solutions, and other localized structures, making them an exciting field of study in nonlinear dynamics and mathematical physics. The term "dispersionless" signifies the lack of a dispersive component [2,3], separating it from the quasi-classical limit of certain ordinary integrable systems, where the dispersive term is eliminated using an appropriate limit [4,5].

Connections to other integrable systems, including the complex short pulse equation [6], which is famous for its loop soliton solutions via hodograph transformation, and the sine-Gordon and Pohlmeyer-Lund-Regge models [3], are shown through the analysis of coupled dispersionless equations. Several facets of CD equations have been studied, such as loop soliton solutions obtained by variable transformations that reveal necessary amplitude conditions for soliton interactions [7]. Higher-order rogue waves and multisoliton solutions have also been discovered for the semi-discrete CD system, highlighting the versatility of the model [8]. Solitons in multicomponent systems have also been studied using the Hirota bilinear technique [9] and Darboux transformation (DT) [10].

Artificial intelligence (AI) now extends beyond laboratory settings into practical applications like manufacturing. Neural networks represent a pivotal subfield within AI. Many scientific publications released annually feature some aspects of AI, especially neural networks, as indicated in Refs. [11–14]. Over the past five years, remarkable progress has been made in leveraging AI for theoretical research in fields such as pure mathematics and theoretical physics [15]. This trend starkly contrasts AI technology's broader reshaping of various human activities over the previous decade [16–18]. Neural networks require training to solve specific problems, with backpropagation serving as the foundational algorithm from which many others have evolved [19–21]. Raissi et al. [22] introduced the physics-informed neural network (PINN) framework for solving nonlinear partial differential equations (PDEs), addressing both forward and inverse problems by embedding physical laws into the loss function. Unlike traditional analytical methods that struggle with complex parameter estimation, neural networks offer a robust alternative. For instance, Wu et al. [23] successfully applied a modified PINN to predict soliton dynamics and model parameters in birefringent fibers. More recently, the bilinear neural network method (BNNM) has emerged as a powerful technique for deriving exact analytical solutions of nonlinear evolution equations (NLEEs), combining the bilinear method with neural network architectures [24–26]. This method has been applied to various models, including the (4+1)-dimensional BLMP-like equation for fluid dynamics [27], integro-differential equations involving interference and soliton solutions [28], and the p-gBKP equation [24]. Furthermore, Zhang and Li [29] proposed a bilinear residual network method to obtain rogue wave solutions, highlighting the versatility and effectiveness of neural network-based approaches in solving complex nonlinear systems.

Among the more advanced techniques is the Levenberg–Marquardt algorithm (LMA), which enhances training efficiency by incorporating aspects of Newton's method [30]. The LMA stands out as a robust optimization method extensively employed in training artificial neural networks (ANNs) for its effectiveness in reducing error functions. This algorithm merges the principles of gradient descent with the Gauss–Newton method, optimizing its suitability for tackling nonlinear least squares challenges. When implemented in ANNs, LMA significantly boosts predictive accuracy and enhances computational speed, as evidenced by multiple research findings [31–33]. Waheed et al. [34] presented novel soliton solutions for a fifth-order nonlinear partial differential equation, the Lax equation, using the exp-function method, and verified these solutions with the LM-ANN, providing a detailed analysis through performance graphs, error histograms, and regression techniques. Riaz et al. [35] investigated the modified Korteweg–de Vries equation in (2+1) dimensions with a time-dependent coefficient, establishing a robust theoretical framework through the identification of the Lax pair and construction of multisoliton solutions via Darboux transformation, then integrated the LM-ANN to train soliton solutions, advancing to the understanding of soliton dynamics and demonstrating their properties through extensive graphical analyses. For more applications of LM-ANN, see the reference within [34,35].

Our work presents an innovative approach using the DT to find analytical solutions for nonlocal CCD equations. In addition, we combine these solutions with the LM-ANN, a neural network framework that enhances the resilience of our outcomes. The combined strategy used in this study facilitates a comprehensive exploration of the dynamics involved, effectively linking theoretical knowledge to practical numerical evaluation. This approach yields fresh insights into systems not extensively analyzed in previous research, thereby shedding light on their complex behaviors and interactions. This methodical exploration gives us a deeper understanding of wave behavior, stability, and non-linear interactions. This enhances our understanding of nonlinear effects and nonlocal dynamics, which are crucial for progressing the field and have implications in physics, engineering, and applied mathematics. Ablowitz et al. in [36] explored the nonzero boundary conditions at infinity for a nonlocal sine-Gordon equation known as the nonlocal CD equation:

$$\rho_t(x,t) + (r(x,t)r(-x,-t))_x = 0, \quad r_{xt}(x,t) = 2r(x,t)\rho(x,t),$$

where $\rho(x,t) = \rho(-x,-t)$. They studied soliton solutions using the inverse scattering method, including one-soliton and two-soliton forms. In this work, we study a reverse space–time nonlocal CCD system:

$$\rho_t(x,t) + \left(r(x,t)r^*(-x,-t)\right)_x = 0, \quad r_{xt}(x,t) - 2\rho(x,t)r(x,t) = 0, \tag{1.1}$$

with $\rho(x,t) = \rho^*(-x,-t)$. The system (1.1) is referred to as a nonlocal complex coupled dispersionless system because it involves complex-valued fields and the nonlocal term $r(x,t)r^*(-x,-t)$, which introduces space–time reflection symmetry. The Lax pair associated with system (1.1) is given by

$$\boldsymbol{\Phi}_x = \zeta \mathbf{A}\boldsymbol{\Phi}, \quad \boldsymbol{\Phi}_t = (\zeta^{-1}\mathbf{J} + \mathbf{B})\boldsymbol{\Phi}, \tag{1.2}$$

where $\boldsymbol{\Phi} = \boldsymbol{\Phi}(x,\ t;\ \zeta)$ is the matrix-valued function that evolves according to the spatial and temporal parts of the Lax representation, with ζ being the spectral parameter, and

$$\mathbf{A} = \mathrm{i}\begin{pmatrix} -\rho(x,t) & -r_x(x,t) \\ -(r^*(-x,-t))_x & \rho(x,t) \end{pmatrix}, \quad \mathbf{J} = \begin{pmatrix} \frac{\mathrm{i}}{2} & 0 \\ 0 & -\frac{\mathrm{i}}{2} \end{pmatrix}, \quad \mathbf{B} = \begin{pmatrix} 0 & -r(x,t) \\ r^*(-x,-t) & 0 \end{pmatrix}.$$

In [37], the authors investigated a nonlocal CCD system (1.1) and derived its DT to obtain multisoliton solutions. They explored various one- and two-soliton and periodic solutions and conducted an asymptotic analysis of these solutions. This study extends the analysis of nonlocal coupled dispersionless systems by integrating DT methods with the LM-ANN. Specifically, we apply LM-ANN to the solutions obtained from the DT, introducing an innovative approach to exploring system dynamics. This integration of machine learning techniques broadens our investigative scope and significantly enhances our results' precision and predictive accuracy, distinguishing our work from previous research. The importance of the obtained results lies in their ability to uncover key aspects of nonlinear wave dynamics and validate analytical solutions through data-driven methods. Below, we outline several contributions that highlight the significance of these findings:

- The solutions describe wave dynamics in a current-fed string under an external magnetic field, highlighting their physical significance.
- Analytical expressions obtained via Darboux transformation provide exact profiles for understanding nonlinear behavior.
- Both symmetry-preserving and non-preserving solutions are explored, revealing a rich structure of possible dynamics.
- Validation through a neural network with the Levenberg–Marquardt algorithm confirms their reliability, even with noisy data.
- Relative L_2 errors and comprehensive visualizations, including surface and contour plots, support the accuracy of results.
- The combined analytical and computational approach bridges theoretical modeling with empirical validation, offering new insights into wave behavior and stability.

The structure of this paper is laid out as follows: Section 1 provides an overview of the CD system, highlights significant past findings, and introduces the (1.1) along with its associated Lax pair. Section 2 discusses the DT and elaborates on deriving the n-fold solutions for the (1.1), represented through simple determinant ratios. Section 3 is dedicated to the computation and analysis of one- and two-soliton solutions against a zero background, utilizing analytical methods and the LM-ANN focusing on relative L_2 error. The paper concludes with Section 4, which summarizes the main findings and proposes potential avenues for future research.

2. Darboux transformation

The exploration of soliton equations has drawn significant attention from researchers employing diverse mathematical strategies. In particular, the inverse scattering method has been investigated by scholars such as Ablowitz et al. [38], Constantin et al. [39], and Pogrebkov [40]. Painlevé analysis has also received considerable attention, with contributions from Ablowitz et al. [38], Liu et al. [41], and Xia et al. [42]. The Bäcklund transformation has been covered in works by Konno and Wadati [43], Yin et al. [44], Luo [45], and Gao [46]. The algebraic geometry approach received attention in work by Belokolos et al. [47], while [48,49] explored the Hirota bilinear form, and similarity transformation is covered in [50]. Among these methods, the DT is thoroughly examined by Matveev and Salle [51]. This technique is celebrated for generating a comprehensive range of analytical solutions, such as breather solutions [52] and rational and rogue wave solutions [53]. The DT's efficacy and versatility make it a key tool for exploring nonlinear phenomena across diverse systems. Recent studies have notably improved the comprehension of coupled dispersionless equations in multiple settings through DT. In [54], matrix-coupled dispersionless equations were introduced, which included the development of a generalized Bäcklund-Darboux transformation and led to obtaining explicit multipole solutions and analyzing their asymptotic behavior. Further, research introduced a matrix-coupled dispersionless system featuring a Lax pair, with solutions expressed using properties of quasideterminants [55]. Another study [56] delved into rogue waves on periodic backgrounds, using the one-fold and two-fold DT to form algebraically decaying solitons and rogue wave solutions derived from Jacobi elliptic functions. DT was further applied to derive various soliton solutions for focusing and defocusing spatial discrete coupled complex short pulse equations [57]. The geometric and algebraic aspects of defocusing complex coupled dispersionless equations in Minkowski space were also examined using the Frenet and Darboux frames [58]. Collectively, these works underscore the DT's versatility and efficiency of DT in producing analytical solutions and studying the dynamics of non-linear systems.

In this section, we introduce the Darboux matrix and construct the DT ($\mathbf{T}$) for the system given by (1.1). This transformation can be defined as

$$\widehat{\boldsymbol{\Phi}} \equiv \mathbf{T}\boldsymbol{\Phi} = (\zeta^{-1} I - \mathbf{M})\boldsymbol{\Phi}, \tag{2.1}$$

where $\mathbf{M}$ is the 2×2 auxiliary matrix. This matrix simplifies the system, allowing us to apply the Lax pair formulation to derive soliton solutions. It includes important interaction terms necessary for analyzing the system (for more details, see [51]). We define[1]

[1] The Darboux transformation can be implemented through two approaches: the inverse matrix and projector method, each with distinct advantages. We use the inverse matrix approach, as defined in (2.1), which uses $\mathbf{M} = \mathbf{H}\mathbf{Z}\mathbf{H}^{-1}$ to update the spectral parameter ζ efficiently, making it ideal for iterative Darboux transformation applications. In contrast, the projector approach, that is, $\widehat{\boldsymbol{\Phi}} = (\zeta - \nu^*)\left(I - \frac{\nu-\nu^*}{\zeta-\mu^*}P\right)$ employs a projector matrix P to selectively modify spectral data, useful in cases like multisoliton interactions where specific modes need emphasis or suppression.

$\mathbf{M}$ as $\mathbf{H}\mathbf{Z}^{-1}\mathbf{H}^{-1}$, with $\mathbf{H}$ representing the specific matrix solution associated with the Lax pair (1.2), and $\mathbf{Z}$ being the diagonal matrix of eigenvalues. The next proposition introduces a fundamental DT for the matrix $\mathbf{A}$ that appears in the spatial part of the Lax pair (1.2). It is important to note that the same results also apply to matrices $\mathbf{J}$ and $\mathbf{B}$.

Proposition 1. *When applying the DT given in (2.1), the new matrix solution $\widehat{\mathbf{A}}$ maintain the same form as $\mathscr{A}$ in (1.2), provided that the matrix $\mathscr{M}$ satisfies the following conditions:*

$$\widehat{\mathbf{A}} = \mathbf{A} - (\mathbf{M})_x\,, \tag{2.2}$$

$$(\mathbf{M})_x\,\mathbf{M} - \mathbf{A}\mathbf{M} + \mathbf{M}\mathbf{A} = 0. \tag{2.3}$$

The proof can be obtained through a simple computation.

Theorem 2.1. *Consider $\mathbf{H}_1, \mathbf{H}_2, \ldots, \mathbf{H}_n$ as particular matrix solutions of the Lax pair defined by (1.2) evaluated at the matrix eigenvalues $\mathbf{Z}_1, \mathbf{Z}_2, \ldots, \mathbf{Z}_n$, respectively. The n-fold iteration of the DT in terms of the inverse matrix can be expressed as follows, with the notation $\mathbf{H}^{(1)} = \mathbf{H}\mathbf{Z}^{-1}$, such that*

$$\mathbf{A}^{[n]} = \mathbf{A} - \left(\sum_{i=1}^{n-1} \mathbf{H}^{(1)}_{[i]}\mathbf{H}^{-1}_{[i]}\right)_x. \tag{2.4}$$

For $\mathbf{H}_k = \begin{pmatrix} X_{2k-1} & X_{2k} \\ Y_{2k-1} & Y_{2k} \end{pmatrix}$ and $\mathbf{Z}_k = \begin{pmatrix} \zeta_{2k-1} & 0 \\ 0 & \zeta_{2k} \end{pmatrix}$, where $k = 1, \ldots, n$, we obtain n-fold solutions to the equation of motion. These solutions are expressed as ratios of simple determinants. The matrices $\mathbf{H}_k$ and $\mathbf{Z}_k$ consist of the functions X_{2k-1}, X_{2k}, Y_{2k-1}, and Y_{2k}, and the eigenvalues ζ_{2k-1} and ζ_{2k} respectively. This formulation simplifies the solution process, making it easier to find the determinant solutions for the scalar components of the system. The n-fold solution $A^{[n]}$ is given by

$$A^{[n]} = A - \left[\frac{1}{|\widehat{\mathbf{H}}|}\begin{pmatrix} \begin{vmatrix} X_1 & \ldots & X_{2n} & 0 \\ Y_1 & \ldots & Y_{2n} & 0 \\ \vdots & & \vdots & \vdots \\ X_1^{(n-1)} & \ldots & X_{2n}^{(n-1)} & 1 \\ Y_1^{(n-1)} & \ldots & Y_{2n}^{(n-1)} & 0 \\ X_1^{(n)} & \ldots & X_{2n}^{(n)} & 0 \end{vmatrix} & \begin{vmatrix} X_1 & \ldots & X_{2n} & 0 \\ Y_1 & \ldots & Y_{2n} & 0 \\ \vdots & & \vdots & \vdots \\ X_1^{(n-1)} & \ldots & X_{2n}^{(n-1)} & 0 \\ Y_1^{(n-1)} & \ldots & Y_{2n}^{(n-1)} & 1 \\ X_1^{(n)} & \ldots & X_{2n}^{(n)} & 0 \end{vmatrix} \\ \begin{vmatrix} X_1 & \ldots & X_{2n} & 0 \\ Y_1 & \ldots & Y_{2n} & 0 \\ \vdots & & \vdots & \vdots \\ X_1^{(n-1)} & \ldots & X_{2n}^{(n-1)} & 1 \\ Y_1^{(n-1)} & \ldots & Y_{2n}^{(n-1)} & 0 \\ Y_1^{(n)} & \ldots & Y_{2n}^{(n)} & 0 \end{vmatrix} & \begin{vmatrix} X_1 & \ldots & X_{2n} & 0 \\ Y_1 & \ldots & Y_{2n} & 0 \\ \vdots & & \vdots & \vdots \\ X_1^{(n-1)} & \ldots & X_{2n}^{(n-1)} & 0 \\ Y_1^{(n-1)} & \ldots & Y_{2n}^{(n-1)} & 1 \\ Y_1^{(n)} & \ldots & Y_{2n}^{(n)} & 0 \end{vmatrix} \end{pmatrix}\right]_x, \tag{2.5}$$

where $X_1^{(1)} = \zeta_1^{-1} X_1$ and

$$|\widehat{\mathbf{H}}| = \begin{vmatrix} X_1 \ldots & X_{2n} & \\ Y_1 & \ldots & Y_{2n} \\ \vdots & & \vdots \\ X_1^{(n-1)} & \ldots & X_{2n}^{(n-1)} \\ Y_1^{(n-1)} & \ldots & Y_{2n}^{(n-1)} \end{vmatrix}.$$

In the next section, we will calculate explicit expressions of one- and two-soliton solutions of the nonlocal CCD system (1.1) on the vanishing background.

3. Explicit solutions

To obtain the explicit solution, we start with the seed solution, defined as

$$r = 0, \qquad \rho = a, \tag{3.1}$$

where a is a constant. This seed solution serves as a starting point for solving the system. The solution $\Phi = \begin{pmatrix} X & Y \end{pmatrix}^{\mathrm{T}}$ to the Lax pair (1.2) using the seed solution (3.1) is given by

$$X = \mathrm{e}^{\mathrm{i}(-\zeta a x + \frac{t}{2\zeta} + A)}, \quad Y = \mathrm{e}^{\mathrm{i}(\zeta a x - \frac{t}{2\zeta} + B)}. \tag{3.2}$$

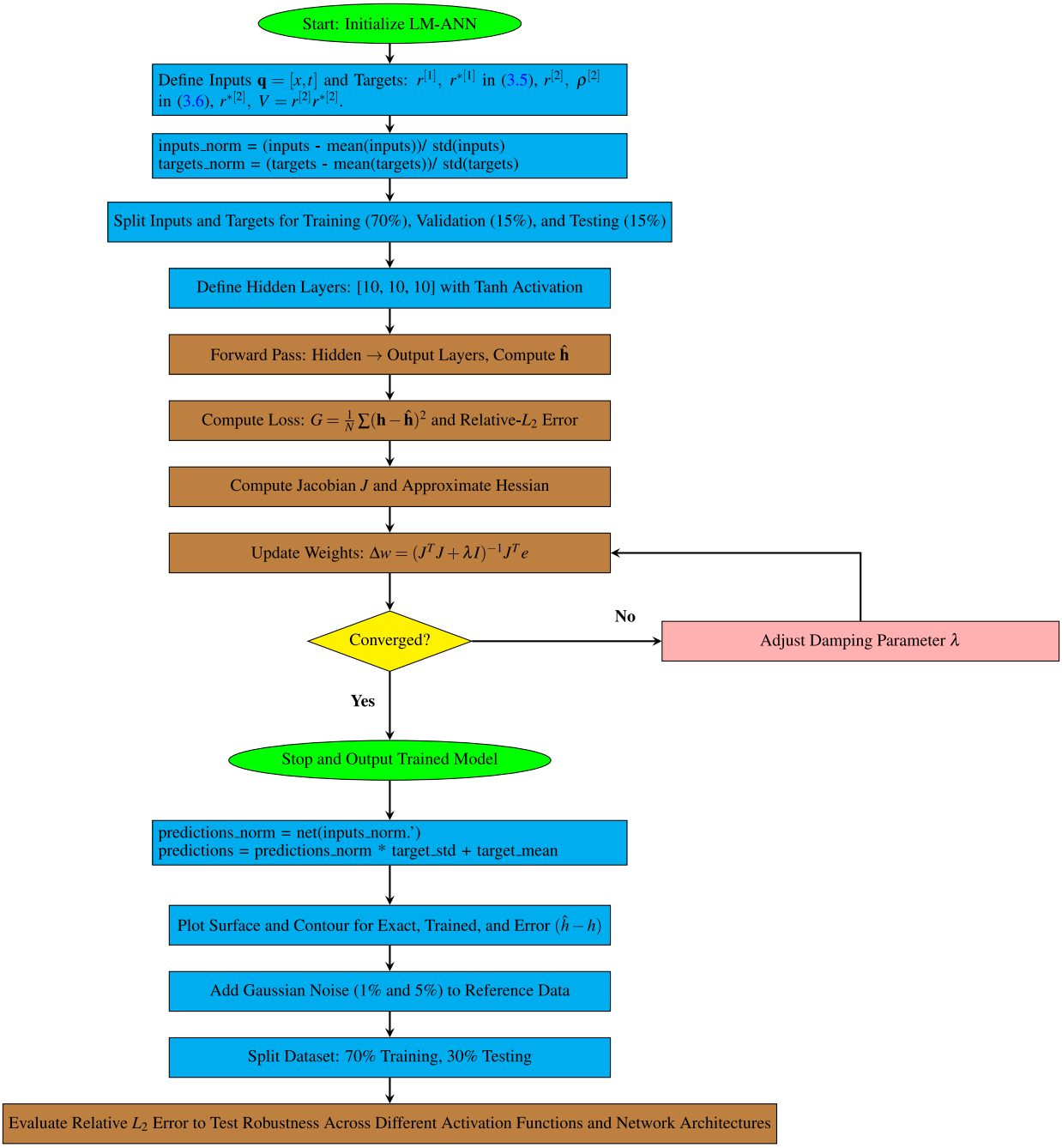

Fig. 1. Flowchart of the LM-ANN framework.

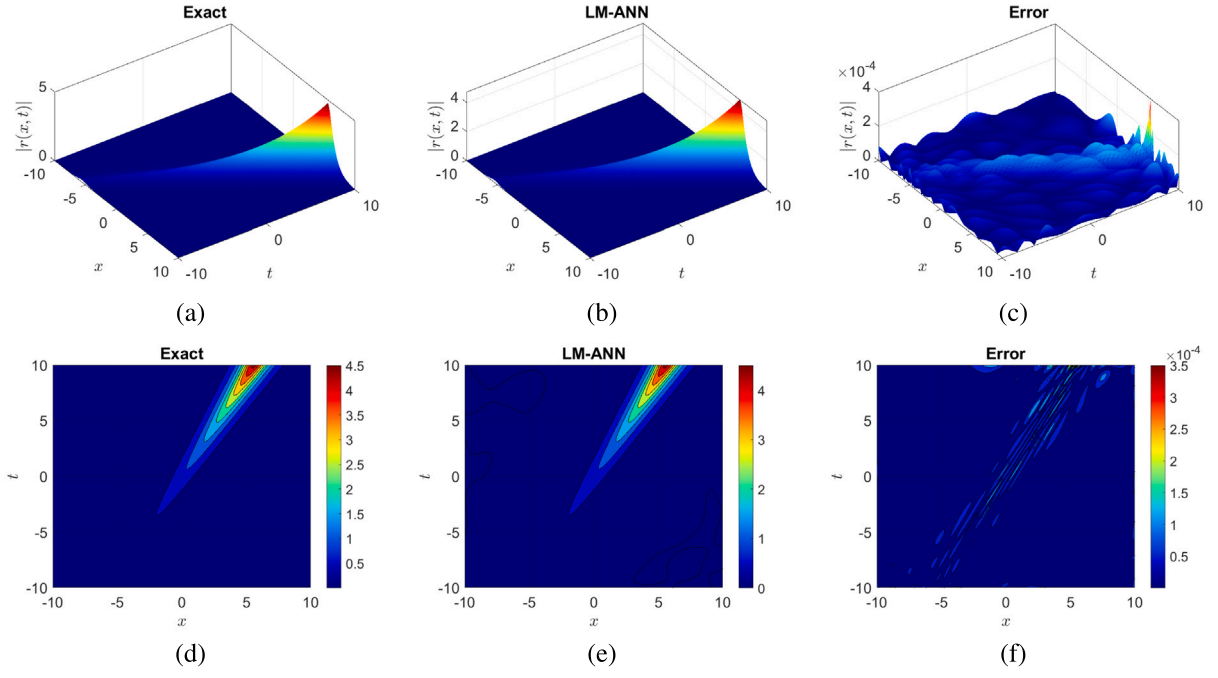

Fig. 2. The profiles of the solution $r^{[1]}$ in Eq. (3.5) are presented for the parameters: $a = -0.5$, $\kappa_1 = 1.2$, $\kappa_2 = 1.5$, $B_1 = 1$, and $B_2 = -1$.

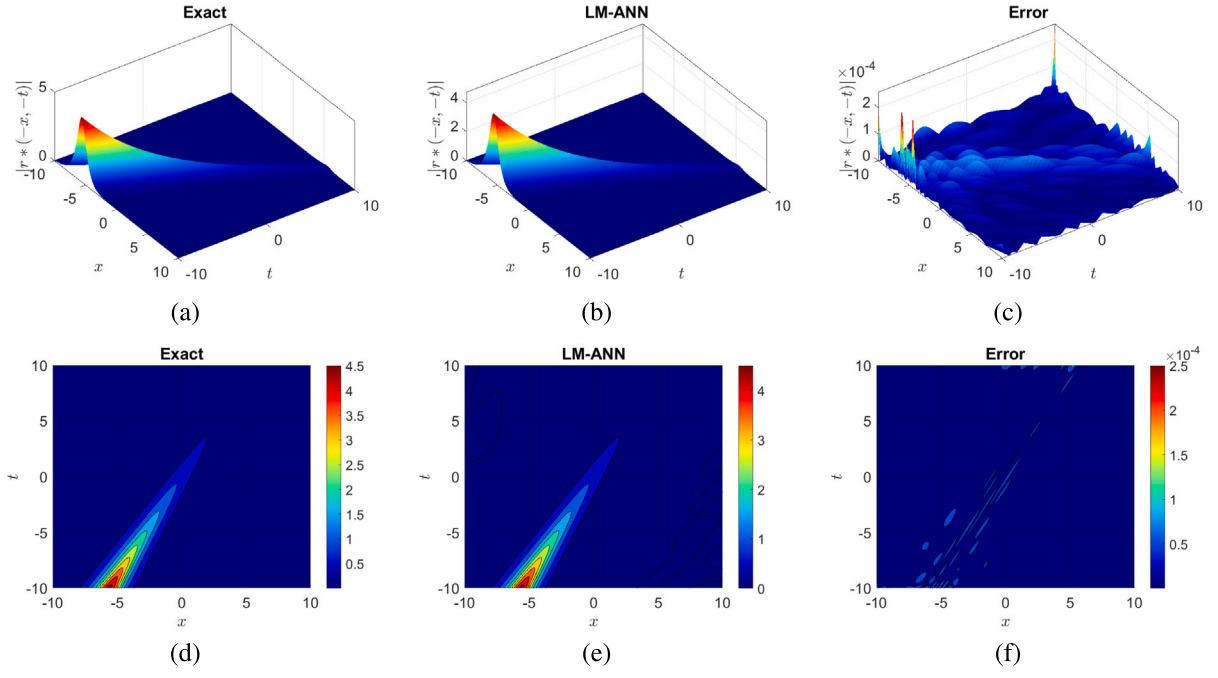

Fig. 3. The profiles of the solution $r^{*[1]}$ in Eq. (3.5) are presented with the same parameters as in Fig. 2.

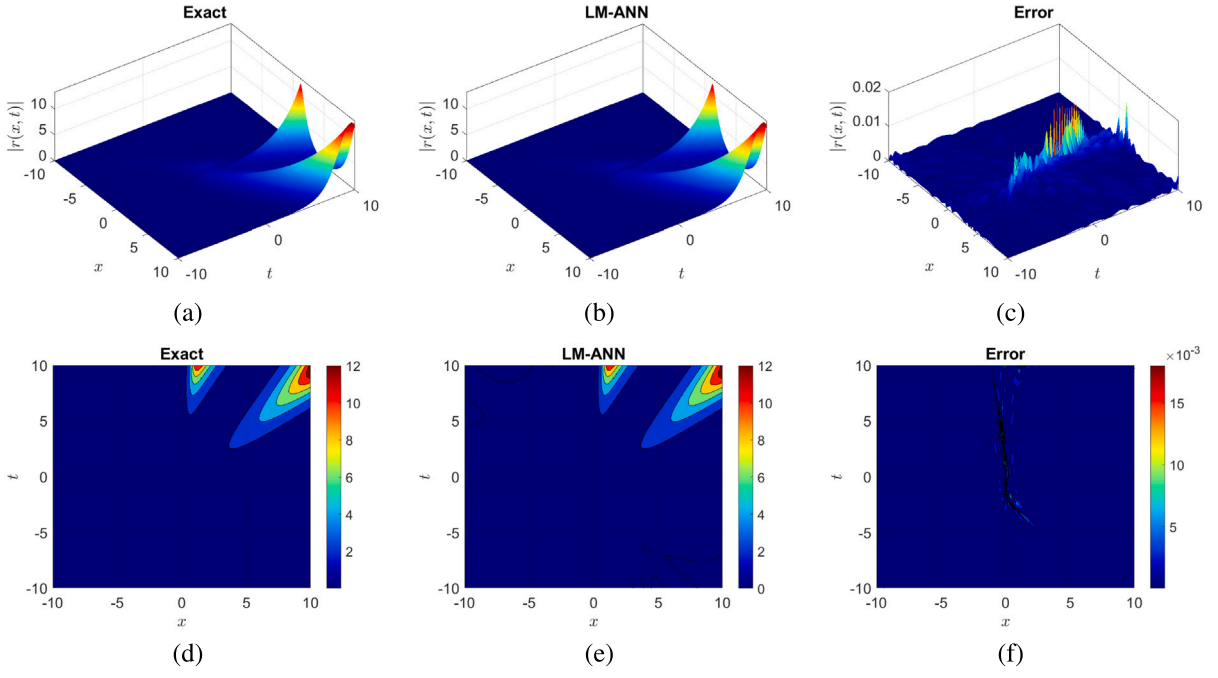

Fig. 4. The solution profiles of $r^{*[2]}$ in Eq. (3.6) are shown for the parameters: $a = -0.25$, $\kappa_1 = 1.2$, $\kappa_2 = 1.8$, $\kappa_3 1.8$, $\kappa_4 = 8.1$, $B_1 = 1.5$, $B_2 = 1$, $B_3 = 1.5$ and $B_4 = 1$.

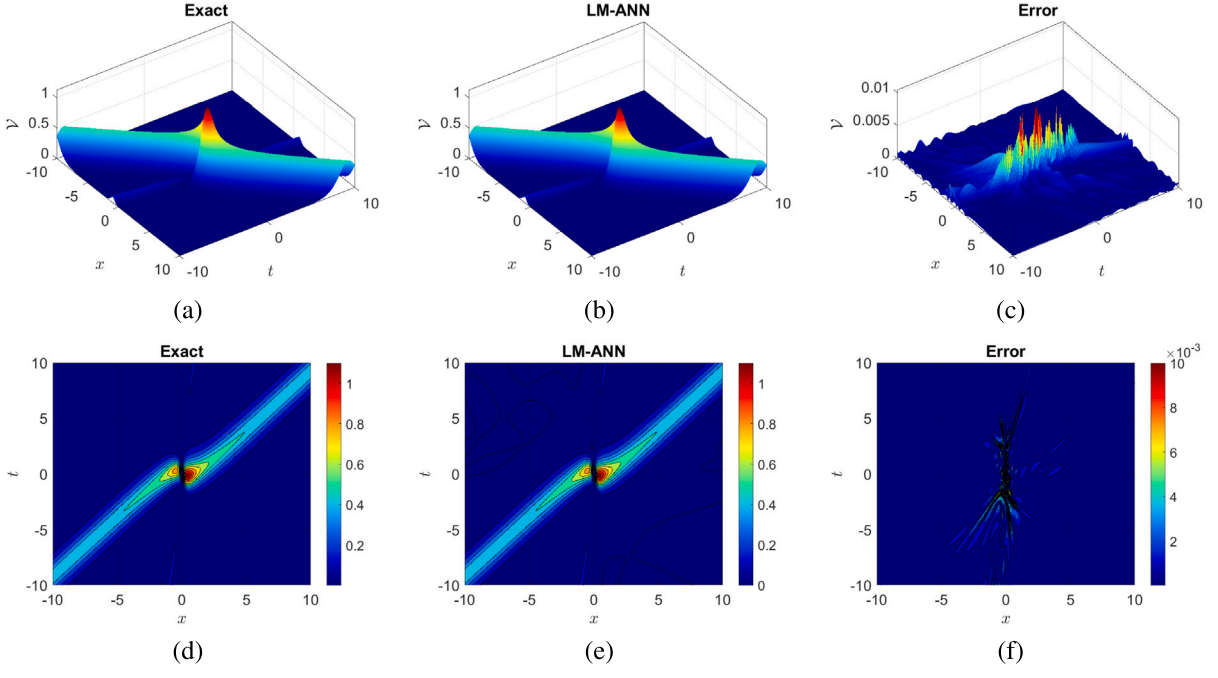

Fig. 5. The solution profiles of $V = r^{[2]}r^{*[2]}$ are shown with the same parameters as in Fig. 4.

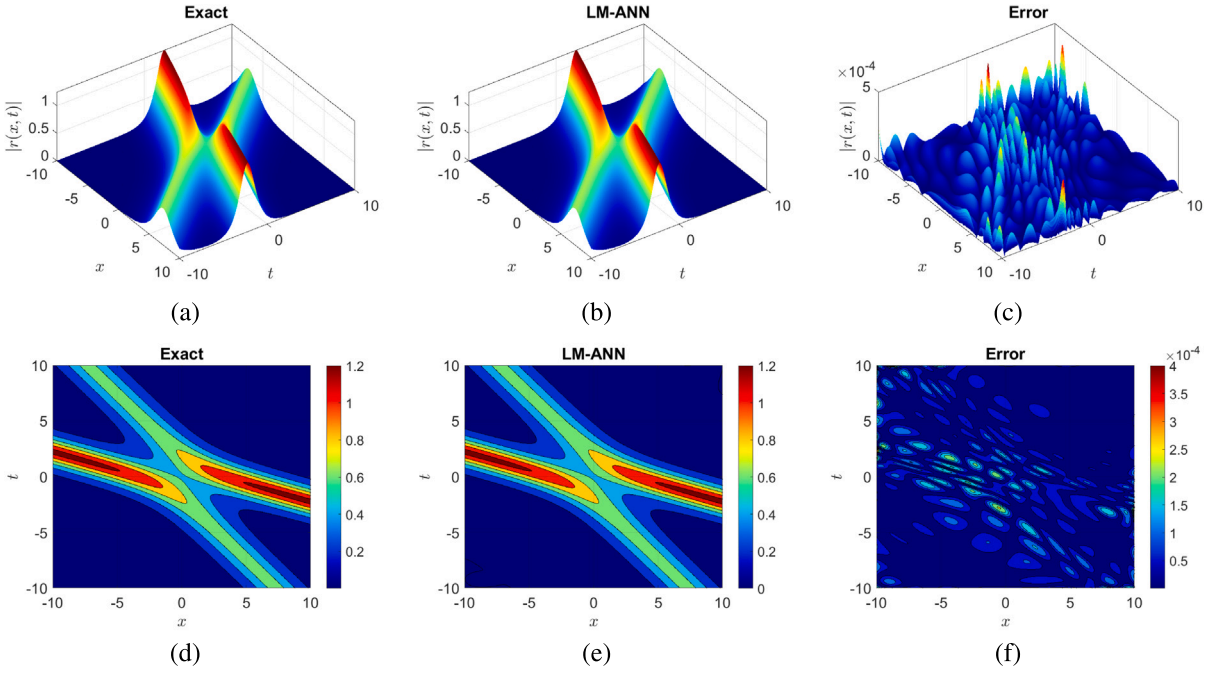

Fig. 6. The profiles of the solution $r^{[2]}$ in Eq. (3.6) are illustrated for the parameters $a = 0.25$, $\kappa_1 = 1.5$, $\kappa_3 = -0.8$, $B_1 = 1.5$, $B_2 = 1$, $B_3 = 1.5$, and $B_4 = 1$.

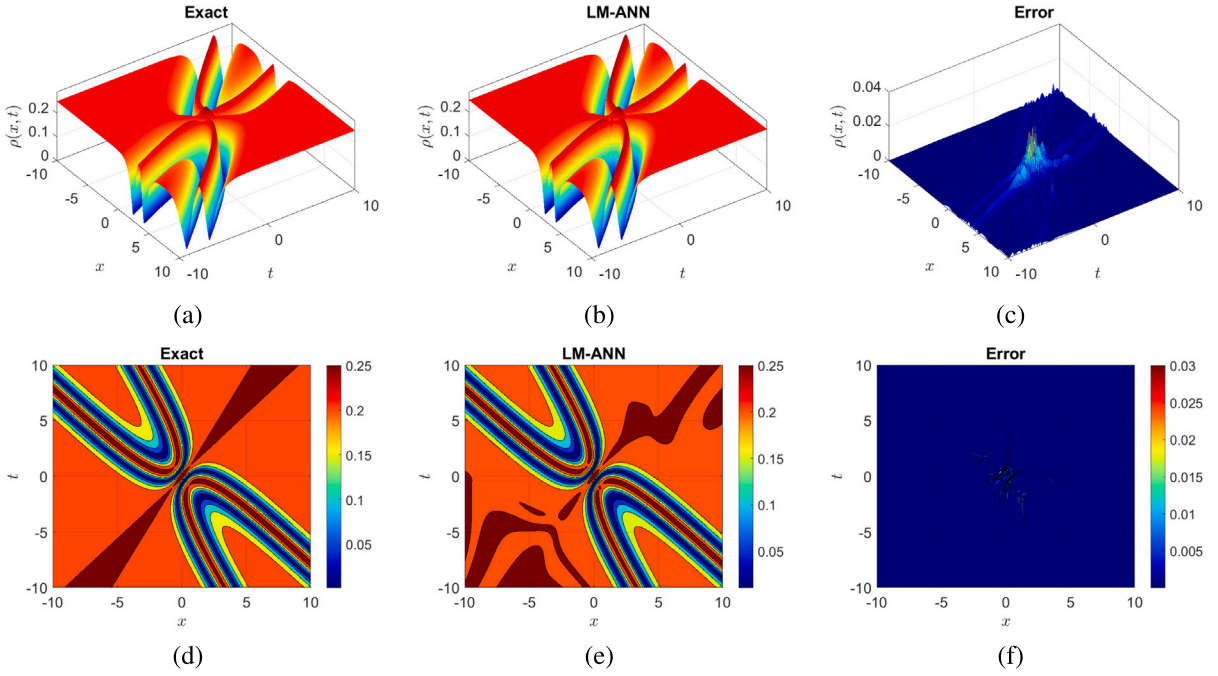

Fig. 7. The profiles of the solution $\rho^{[2]}$ in Eq. (3.6) are illustrated for the parameters $a = 0.25$, $\kappa_1 = 1.2$, $\kappa_2 = 1.8$, $\kappa_3 1.8$, $\kappa_4 = 2.1$, $B_1 = 1.5$, $B_2 = 1$, $B_3 = 1.5$ and $B_4 = 1$.

In (3.2) A and B are real constants. Since the system (1.1) is expressed in terms of the fields ρ and r, expressing the determinant solutions for these fields is more appropriate. Therefore, we can express $\rho^{[n]}$ and $r^{[n]}$, derived from (2.5), in the following form

$$\rho^{[n]} = \rho + \mathrm{i}\left[\frac{1}{|\widehat{\mathbf{H}}|}\begin{vmatrix} X_1 & \dots & X_{2n} & 0 \\ Y_1 & \dots & Y_{2n} & 0 \\ \vdots & & \vdots & \vdots \\ X_1^{(n-1)} & \dots & X_{2n}^{(n-1)} & 1 \\ Y_1^{(n-1)} & \dots & Y_{2n}^{(n-1)} & 0 \\ X_1^{(n)} & \dots & X_{2n}^{(n)} & 0 \end{vmatrix}\right]_x, \quad r^{[n]} = r + \mathrm{i}\left[\frac{1}{|\widehat{\mathbf{H}}|}\begin{vmatrix} X_1 & \dots & X_{2n} & 0 \\ Y_1 & \dots & Y_{2n} & 0 \\ \vdots & & \vdots & \vdots \\ X_1^{(n-1)} & \dots & X_{2n}^{(n-1)} & 0 \\ Y_1^{(n-1)} & \dots & Y_{2n}^{(n-1)} & 1 \\ X_1^{(n)} & \dots & X_{2n}^{(n)} & 0 \end{vmatrix}\right]. \tag{3.3}$$

In what follows, we will explicitly compute the one-soliton ($n = 1$) solutions. These solutions are derived under the following reductions: $\zeta_1 = \mathrm{i}\kappa_1, \quad \zeta_2 = -\mathrm{i}\kappa_2, \quad A_1 = -B_1, \quad A_2 = B_2$, where $\kappa_1 \neq \kappa_2$ are real constants. With these reductions, they maintain a symmetric structure. Hence, we have

$$\rho^{[1]} = a - \frac{2a(\kappa_1+\kappa_2)^2}{\kappa_1\kappa_2\left[2\sinh\left(\theta_1 - \mathrm{i}B_1\right)\right]^2}, \tag{3.4}$$

$$r^{[1]} = -\frac{(\kappa_1+\kappa_2)\,e^{\theta_2+\mathrm{i}(-B_1)}}{\kappa_1\kappa_2\left[2\sinh(\theta_1 - \mathrm{i}B_1)\right]}, \quad r^{*[1]} = \frac{(\kappa_1+\kappa_2)\,e^{-\theta_2+i(B_1)}}{\kappa_1\kappa_2\left[2\sinh(\theta_1 - \mathrm{i}B_1)\right]}, \tag{3.5}$$

where

$$\theta_1 = \frac{2ax\kappa_1^2\kappa_2 + \left(2ax\kappa_2^2 + t\right)\kappa_1 + t\kappa_2}{2\kappa_1\kappa_2}, \quad \theta_2 = \frac{2ax\kappa_1^2\kappa_2 + \left(-2ax\kappa_2^2 - t\right)\kappa_1 + t\kappa_2}{2\kappa_1\kappa_2}.$$

The spectral parameters are carefully chosen to ensure that the dynamical variables preserve the nonlocal symmetry. This allows the two solutions, given in (3.5), to be related to each other through parity, time reversal, and complex conjugation. The profiles of symmetry-preserving soliton solutions (3.5) for nonlocal CCD system (1.1) are shown in Figs. 2 and 3. The solution (3.4) represents the structure of the dark soliton. It can be observed that the behavior of $r^{[1]}$ and $r^{*[1]}$ evaluated at $(x,\ t)$ and $(-x,\ -t)$ respectively is driven by their exponential terms. Specifically, the terms $\mathrm{e}^{2ax\kappa_1^2}$ in $r^{[1]}$ and $\mathrm{e}^{-2ax\kappa_1^2}$ in $r^{*[1]}$ are responsible for growth and decay, respectively. As x and t increase, the exponential in $r^{[1]}$ leads to growth, while the exponential in $r^{*[1]}$, evaluated at $-x$ and $-t$, causes decay. These terms reflect the energy balance in soliton solutions, with one solution expanding while the other decays. It is this dynamic nature that is captured in the solution having localized and evolving solitons. If the exponential terms were removed, the solutions would no longer retain their characteristic growth and decay to uniform wave profile with a loss of dynamic interaction between the solitons. Without exponential terms, the solution would not have the energy exchange defining the growth of one solution and the decay of the other. This would decrease the interaction and localization of the soliton in space–time and could yield a static or less dynamic wave pattern. If $a = 0$, the exponential growth and decay terms vanish, but $r^{[1]}$ and $r^{*[1]}$ are individually non-trivial. Each solution takes on a distinct, well-defined form, even when the spatial terms are absent. This is further supported by the product $V = r^{[1]}(x,t)r^{*[1]}(-x,-t)$ because it gives rise to a combined structure that remains localized in time and thus indeed supports a temporal soliton. In other words, while the spatial growth and decay terms are eliminated, the solution keeps its solitonic character manifesting itself in the form of the time-localized pulse with non-trivial features both in $r^{[1]}$ and $r^{*[1]}$ individually as well as in their product.

In what follows, we derive two-soliton solutions to examine how solitons interact within a nonlocal system. Such interactions are crucial for understanding non-linear wave behavior as they reveal important aspects of wave stability and persistence under nonlocal effects. Studying two-soliton solutions is relevant in fields like ferromagnetism, optical fibers, and other disciplines, where soliton collisions can significantly affect energy transfer, structural changes, and the overall dynamics of nonlinear systems. For $n = 2$, the solutions $\rho^{[2]}$ and $r^{[2]}$ with the seed solution (3.1) have the following form

$$\rho^{[2]} = a + \frac{\mathrm{i}}{\widehat{\mathbf{H}}_2}\begin{vmatrix} X_1 & X_2 & X_3 & X_4 & 0 \\ Y_1 & Y_2 & Y_3 & Y_4 & 0 \\ \frac{X_1}{\zeta_1} & \frac{X_2}{\zeta_2} & \frac{X_3}{\zeta_3} & \frac{X_4}{\zeta_4} & 1 \\ \frac{Y_1}{\zeta_1} & \frac{Y_2}{\zeta_2} & \frac{Y_3}{\zeta_3} & \frac{Y_4}{\zeta_4} & 0 \\ \frac{X_1}{\zeta_1^2} & \frac{X_2}{\zeta_2^2} & \frac{X_3}{\zeta_3^2} & \frac{X_4}{\zeta_4^2} & 0 \end{vmatrix}, \quad r^{[2]} = \frac{\mathrm{i}}{\widehat{\mathbf{H}}_2}\begin{vmatrix} X_1 & X_2 & X_3 & X_4 & 0 \\ Y_1 & Y_2 & Y_3 & Y_4 & 0 \\ \frac{X_1}{\zeta_1} & \frac{X_2}{\zeta_2} & \frac{X_3}{\zeta_3} & \frac{X_4}{\zeta_4} & 0 \\ \frac{Y_1}{\zeta_1} & \frac{Y_2}{\zeta_2} & \frac{Y_3}{\zeta_3} & \frac{Y_4}{\zeta_4} & 1 \\ \frac{X_1}{\zeta_1^2} & \frac{X_2}{\zeta_2^2} & \frac{X_3}{\zeta_3^2} & \frac{X_4}{\zeta_4^2} & 0 \end{vmatrix}, \tag{3.6}$$

where

$$\widehat{\mathbf{H}}_2 = \begin{vmatrix} X_1 & X_2 & X_3 & X_4 \\ Y_1 & Y_2 & Y_3 & Y_4 \\ \frac{X_1}{\zeta_1} & \frac{X_2}{\zeta_2} & \frac{X_3}{\zeta_3} & \frac{X_4}{\zeta_4} \\ \frac{Y_1}{\zeta_1} & \frac{Y_2}{\zeta_2} & \frac{Y_3}{\zeta_3} & \frac{Y_4}{\zeta_4} \end{vmatrix}.$$

For the parameters $\zeta_1 = \mathrm{i}\kappa_1$, $\zeta_2 = -\mathrm{i}\kappa_2$, $A_1 = -B_1$, $A_2 = B_2$, $\zeta_3 = \mathrm{i}\kappa_3$, $\zeta_4 = -\mathrm{i}\kappa_4$, $A_3 = -B_3$, and $A_4 = B_4$, the solution is said to be symmetrically preserved. This configuration results in different behaviors for $r^{[2]}(x,\ t)$ and $r^{*[2]}(-x,\ -t)$: the structure of $r^{[2]}(x,\ t)$

represents the interaction of two growing solitons (see Fig. 4), while $r^{*[2]}(-x,\ -t)$ exhibits the decay of two solitons. In particular, the product $V = r^{[2]}(x,\ t)r^{*[2]}(-x,\ -t)$ demonstrates the interaction of two stable solitons as seen in Fig. 5, a phenomenon that underscores the unique characteristics of the nonlocal system. In the nonlocal case, such an interaction allows for sustained stability over time, essential for applications requiring long-term soliton persistence. Furthermore, the structure of $q^{[2]}$ shows interactions of two dark solitons as depicted in Fig. 7, revealing the presence of dark soliton solutions in the nonlocal regime. Dark solitons in nonlocal systems provide information on phase shifts and wave cancellations, which are relevant for various physical applications.

However, when the parameters are modified to $\zeta_1 = \mathrm{i}\kappa_1$, $\zeta_2 = -\mathrm{i}\kappa_1$, $A_1 = -B_1$, $A_2 = B_2$, $\zeta_3 = \mathrm{i}\kappa_3$, $\zeta_4 = -\mathrm{i}\kappa_3$, $A_3 = -B_3$, and $A_4 = B_4$, we observe the interaction of two bright solitons. This case, where $\kappa_1 = \kappa_2$ and $\kappa_3 = \kappa_4$, leads to a solution that is not symmetrically preserved, as seen in the classical system. In this case, the lack of symmetry leads to solitons not exhibiting the self-sustaining, non-decaying properties observed in a nonlocal system. This highlights the unique behaviors that symmetry preservation introduces in nonlocal systems compared to the classical context. These findings are illustrated in Fig. 6, which visualizes the interactions between two bright solitons. The two-soliton solutions describe the elastic interaction of two individual solitons, where two distinct lumps of energy, moving at different velocities, interact and scatter without altering their shapes. By applying DT repeatedly to the seed solution, explicit expressions for higher-order multi-solitons can be derived. For example, a three-soliton configuration models the scattering of three solitons with different amplitudes. The characteristics of multisoliton configurations in local and nonlocal CCD systems can be further investigated and compared with their discrete counterparts, where one or both independent variables are discretized. More complex multisoliton solutions, such as breather and rogue wave solutions, can also be obtained using the DT. In the asymptotic limit, the multisoliton configuration factorizes into single n solitons, a behavior that becomes apparent when the asymptotic limit is taken.

3.1. Levenberg–Marquardt artificial neural network

The Levenberg–Marquardt (LM) algorithm is a supervised training technique used to optimize weights in feedforward neural networks. A conventional neural network comprises several layers, each containing a limited number of neurons. The output layer is essential for generating the network's results. Prior levels, referred to as hidden layers, facilitate input processing by modifying data through a sequence of computations. Feedforward neural networks, such as the widely utilized multilayer perceptron (MLP), exhibit a sequential architecture in which each layer is exclusively connected to the subsequent layer. Modifiable synaptic weights connect neurons within these layers [59], essential for the network's learning mechanism. Throughout training, the algorithm modifies these weights according to the input and expected output to reduce errors, enhancing the network's efficacy. Initially, weights are randomly assigned and have no inherent significance unless they are optimized through training [60].

The network architecture examined in the study is such that $\mathbf{q}$ contained values for the input variable. The input variable is associated with each of N neurons in a hidden layer (**HL**) by using weights $(\mathbf{w}_i;\quad i = 1, 2, \ldots, N)$. Following [61], the mapping has two forms for the relationship between output $\hat{\mathbf{h}}$ and input variable:

$$\mathrm{HL}_i^{(1)} = \mathbf{w}_i^{(1)}\mathbf{q} + \mathbf{b}_i^{(1)};\quad \mathbf{e}_i^{(1)} = \mathbf{g}_{\mathrm{l}1}(\mathrm{HL}_k^{(1)}),$$

$$\mathrm{OL}_i^{(2)} = \mathbf{w}_i^{(2,1)}\mathbf{q} + \mathbf{b}_i^{(1)},\quad \hat{\mathbf{h}} = \mathbf{e}_i^{(2)} = \mathbf{g}_{\mathrm{l}2}(\mathrm{HL}_k^{(2)}).$$

For a neural network with N neurons, initial biases are denoted by $\mathbf{b}_1^{(1)}, \mathbf{b}_2^{(1)}, \ldots, \mathbf{b}_N^{(1)}$. Before activation, the input to each neuron k is the sum of $\mathbf{b}_k^{(1)}$ and the weighted inputs $\mathbf{w}_k\mathbf{q}$. An activation function, which could be either linear or nonlinear, designated as $\mathbf{g}(\cdot)$, modifies this input in each neuron, resulting in $\mathbf{g}_k\left(\mathbf{b}_k^{(1)} + \mathbf{w}_k\mathbf{q}\right) = \mathbf{g}_k\left(n_k^{(1)}\right)$, for $k = 1, 2, \ldots, N$. Once activated, these values are passed to the output layer (**OL**), cumulatively expressed as $\sum_{k=1}^{N}\mathbf{w}_k'\mathbf{g}_k\left(\mathbf{b}_k^{(1)} + \mathbf{w}_k\mathbf{q}\right) + \mathbf{b}^{(2)}$, with $\mathbf{w}_k = (k = 1, 2, \ldots, N)$ representing the bias parameters in both the hidden and output layers. This transformed output is then processed by another function $\mathbf{f}(\cdot)$, leading to $\mathbf{f}\left(\sum_{k=1}^{N}\mathbf{w}_k'\mathbf{g}_k(.) + \mathbf{b}^{(2)}\right) = \mathbf{g}_k\left(n_k^{(2)}\right)$. This output subsequently estimates the target variable $\hat{\mathbf{h}}$ for the training dataset or $\mathbf{h}$:

$$\hat{\mathbf{h}} = \mathbf{f}\left(\sum_{k=1}^{N}\mathbf{w}_k'\mathbf{g}\left(\mathbf{w}_k\mathbf{q} + \mathbf{b}_k^{(1)}\right) + \mathbf{b}^{(2)}\right).\quad k = 1, 2, \ldots, N$$

To train the solutions $r^{[1]}$, $r^{*[1]}$, in (3.5), $r^{[2]}$, $\rho^{[2]}$ in (3.6), $r^{*[2]}$, and $V = r^{[2]}r^{*[2]}$, using the LM-ANN, we divide the data into two parts: 70% of the organized dataset is used for training, and the remaining 30% is used for testing. In all solutions, the variables x and t are considered input variables. A commonly used performance metric measures the difference between actual and predicted data during the model training phase, articulated as follows:

$$G = K_U(U, P) = \frac{1}{N}\sum_{i=1}^{n}(\mathbf{h}_i - \hat{\mathbf{h}}_i)^2,$$

where K_U denotes the average of squared deviations, reflecting network errors; U corresponds to the training data of paired inputs and targets; and P describes the neural network's structure, including the number of layers, the number of units in each, and the type of activation function. K_U plays a critical role in activating early stopping mechanisms to prevent overfitting and is widely

Table 1
Solution $r^{[1]}$ in (3.5): Model performance with clean and noisy data for $t = 0.5$. Refer to Fig. 2.

Activation	No of nodes	Clean data (Relative L_2 error)		Noise data (Relative L_2 error)			
function	in each HL	Trained	Testing	Trained (1% Noise)	Testing (1% Noise)	Trained (5% Noise)	Testing (5% Noise)
tanh	[5, 5, 5]	8.4729e−08	1.4909e−07	0.00033732	0.00059323	0.0017174	0.0031362
tanh	[10, 10, 10]	1.4886e−07	2.7043e−07	0.0003345	0.00061294	0.0017704	0.0027553
tanh	[20, 20, 20]	7.6309e−07	1.4911e−06	0.0003079	0.00068087	0.0019583	0.002557
tanh	[5, 5, 5, 5]	1.4739e−07	2.7297e−07	0.00032791	0.00061335	0.0018462	0.0027322
tanh	[10, 10, 10, 10]	3.3562e−07	6.5454e−07	0.00032279	0.00066367	0.0019268	0.0026621
tanh	[20, 20, 20, 20]	2.9657e−07	5.3123e−07	0.00034128	0.00053372	0.0018002	0.002547
sigmoid	[5, 5, 5]	8.3347e−07	1.453e−06	0.00034082	0.00053593	0.0018704	0.0024503
sigmoid	[10, 10, 10]	1.2928e−06	1.9787e−06	0.00032578	0.00071692	0.0017614	0.0030593
sigmoid	[20, 20, 20]	7.0481e−07	1.4568e−06	0.00032889	0.00055222	0.0021325	0.0028303
sigmoid	[5, 5, 5, 5]	5.2121e−07	9.4023e−07	0.0003541	0.00054816	0.0017959	0.0017959
sigmoid	[10, 10, 10, 10]	1.9426e−07	2.5936e−07	0.00030426	0.00063301	0.0018541	0.0026543
sigmoid	[20, 20, 20, 20]	7.7554e−07	1.3264e−06	0.0003441	0.00055538	0.0019102	0.0019102

Table 2
Solution $r^{*[1]}$ in (3.5): Model performance with clean and noisy data for $t = 0.5$.

Activation	No of nodes	Clean data (Relative L_2 error)		Noise data (Relative L_2 error)			
function	in each HL	Trained	Testing	Trained (1% Noise)	Testing (1% Noise)	Trained (5% Noise)	Testing (5% Noise)
tanh	[5, 5, 5]	1.7654e−06	2.8164e−06	0.00036827	0.00055543	0.0018268	0.0030727
tanh	[10, 10, 10]	2.6111e−06	4.4766e−06	0.00035669	0.00059653	0.0018138	0.0033708
tanh	[20, 20, 20]	3.0556e−06	6.0053e−06	0.00036974	0.00062545	0.0016929	0.0030196
tanh	[5, 5, 5, 5]	3.1486e−06	5.4751e−06	0.00034812	0.00056264	0.0018499	0.002857
tanh	[10, 10, 10, 10]	2.0005e−06	3.8793e−06	0.00037552	0.00060913	0.0017759	0.0034193
tanh	[20, 20, 20, 20]	1.7582e−06	2.9307e−06	0.00037503	0.00058248	0.0018411	0.0027667
sigmoid	[5, 5, 5]	4.2248e−06	1.453e−06	0.00034422	0.00053593	0.0018193	0.0025366
sigmoid	[10, 10, 10]	1.4297e−06	2.6714e−06	0.00034733	0.00052253	0.0019086	0.0029701
sigmoid	[20, 20, 20]	4.5782e−06	8.0543e−06	0.0003608	0.00054468	0.0017619	0.0023565
sigmoid	[5, 5, 5, 5]	5.4047e−06	7.8359e−06	0.00039218	0.0005756	0.0017828	0.0035557
sigmoid	[10, 10, 10, 10]	5.2915e−06	8.9121e−06	0.0003714	0.00060505	0.0017263	0.0028074
sigmoid	[20, 20, 20, 20]	7.7554e−07	1.3264e−06	0.00035477	0.00051751	0.0017269	0.0030786

used in MATLAB training routines. For the complete procedure of LM-ANN, see the flowchart in Fig. 1. To evaluate the solution's performance as predicted by LM-ANN, we calculate the relative L_2 error as:

$$\text{Relative-}L_2 = \frac{\sqrt{\text{MSE}}}{\sqrt{\sum_i h_i^2}}.$$

The network is designed with three hidden layers, each containing ten nodes, and employs hyperbolic tangent activation functions to handle non-linear patterns effectively. After training, the network's predictions are compared to the exact values, and the differences (errors) are analyzed. The exact solutions (see Figs. 2(a), 3(a), 4(a), 5(a), 6(a), 7(a), 2(d), 3(d), 4(d), 5(d), 6(d), and 7(d)), neural network predictions (see Figs. 2(b), 3(b), 4(b), 5(b), 6(b), 7(b), 2(e), 3(e), 4(e), 5(e), 6(e), and 7(e)), and errors (see Figs. 2(c), 3(c), 4(c), 5(c), 6(c), 7(c), 2(f), 3(f), 4(f), 5(f), 6(f), and 7(f)) are visualized using 3D surface and contour plots, demonstrating the network's ability to approximate the solutions $r^{[1]}$, $r^{*[1]}$, in (3.5), $r^{[2]}$, $\rho^{[2]}$ in (3.6), $r^{*[2]}$, and $V = r^{[2]}r^{*[2]}$, accurately and reliably. Furthermore, we use a neural network with multiple layers, each containing varying numbers of nodes, to model the solutions of (1.1). The network employs various activation functions in the hidden layers to effectively capture the non-linear patterns in the data. We also add Gaussian noise to the target data to make the training process more realistic. The network is trained using the LM-ANN method for up to ten iterations to avoid overtraining and improve accuracy. The training stops if a certain quality is reached, the maximum number of iterations is exceeded, or other stopping criteria are met. The network's performance is measured using the relative L_2 errors, as shown in Tables 1, 2, 3, 4, 5, and 6 for $t = 0.5$. These tables compare the predicted solutions to the exact solutions, including $r^{[1]}$, $r^{*[1]}$, $r^{*[2]}$, $\rho^{[2]}$, and $V = r^{[2]}r^{*[2]}$. The results show that the network performs well, with predictions closely matching the exact solutions, proving its effectiveness and reliability in modeling complex behaviors.

4. Concluding remarks

This study provides an in-depth analysis of the nonlocal CCD system, employing theoretical and neural network approaches to derive and validate soliton solutions. Using the Darboux transformation, we obtained analytical solutions represented by simple determinant ratios, focusing on symmetry-preserving and non-preserving soliton solutions. Our findings reveal that when spectral parameters are chosen without coherent relations, the dynamical variables yield complex-valued potential terms, resulting in non-preserving symmetry solutions. In contrast, parameter choices with coherent relationships lead to symmetric dynamical variables and symmetry-preserving solutions. Furthermore, we enhanced and verified these solutions by implementing the Levenberg–Marquardt

Table 3
Solution $r^{*[2]}$: Model performance with clean and noisy data for $t = 0.5$.

Activation	No of nodes	Clean data (Relative L_2 error)		Noise data (Relative L_2 error)			
function	in each HL	Trained	Testing	Trained (1% Noise)	Testing (1% Noise)	Trained (5% Noise)	Testing (5% Noise)
tanh	[5, 5, 5]	2.7227e−06	4.4809e−06	0.00028677	0.00046886	0.0015395	0.002341
tanh	[10, 10, 10]	1.6311e−06	2.9171e−06	0.0003123	0.00047046	0.001566	0.0022733
tanh	[20, 20, 20]	2.3846e−06	5.355e−06	0.00030507	0.00045438	0.0016239	0.0022741
tanh	[5, 5, 5, 5]	2.4618e−06	4.4232e−06	0.00029342	0.00039213	0.0015411	0.0023353
tanh	[10, 10, 10, 10]	1.2968e−06	2.4799e−06	0.00031503	0.00046439	0.001521	0.0025139
tanh	[20, 20, 20, 20]	2.2485e−06	5.0339e−06	0.00029566	0.00046686	0.0015628	0.0021857
sigmoid	[5, 5, 5]	1.8872e−06	2.898e−06	0.00031142	0.00048858	0.0015167	0.002507
sigmoid	[10, 10, 10]	1.5551e−06	2.6766e−06	0.00033158	0.00042895	0.001545	0.0024539
sigmoid	[20, 20, 20]	2.2946e−06	4.4904e−06	0.0003115	0.00045137	0.0015096	0.002309
sigmoid	[5, 5, 5, 5]	1.3658e−06	2.675e−06	0.00031846	0.0004486	0.0014893	0.0024307
sigmoid	[10, 10, 10, 10]	5.2915e−06	8.9121e−06	0.0003714	0.00060505	0.0015971	0.0024695
sigmoid	[20, 20, 20, 20]	2.3157e−06	4.7955e−06	0.00030517	0.00043517	0.00156	0.0023748

Table 4
Solution $V = r^{[2]}r^{*[2]}$: Model performance with clean and noisy data for $t = 0.5$.

Activation	No of nodes	Clean data (Relative L_2 error)		Noise data (Relative L_2 error)			
function	in each HL	Trained	Testing	Trained (1% Noise)	Testing (1% Noise)	Trained (5% Noise)	Testing (5% Noise)
tanh	[5, 5, 5]	5.397e−05	0.00011702	0.00033138	0.00060537	0.0016744	0.0030827
tanh	[10, 10, 10]	0.00016905	0.00031178	0.00038545	0.00059186	0.0016635	0.0027755
tanh	[20, 20, 20]	2.0645e−06	5.2314e−06	0.00035613	0.00047847	0.0018082	0.0027576
tanh	[5, 5, 5, 5]	0.00037186	0.00059648	0.00032237	0.000605	0.0016826	0.0028983
tanh	[10, 10, 10, 10]	0.00021088	0.00023458	0.00041407	0.00057393	0.0016758	0.0024823
tanh	[20, 20, 20, 20]	1.4793e−06	9.1648e−05	0.00035142	0.00050362	0.0017843	0.0024369
sigmoid	[5, 5, 5]	0.00079593	0.0011571	0.00089993	0.0010604	0.0016273	0.0025847
sigmoid	[10, 10, 10]	2.4259e−06	1.2524e−05	0.00034922	0.00047839	0.0017003	0.0022386
sigmoid	[20, 20, 20]	2.1089e−06	2.325e−05	0.00033757	0.00055142	0.0017051	0.0026508
sigmoid	[5, 5, 5, 5]	0.00018835	0.00028656	0.0003828	0.00055376	0.001865	0.0027416
sigmoid	[10, 10, 10, 10]	3.8072e−06	1.5634e−05	0.00037025	0.00052723	0.001797	0.0027272
sigmoid	[20, 20, 20, 20]	1.4196e−05	2.5897e−05	0.00036477	0.000559	0.0017467	0.0030069

Table 5
Solution $r^{[2]}$ in (3.6): Model performance with clean and noisy data for $t = 0.5$.

Activation	No of nodes	Clean data (Relative L_2 error)		Noise data (Relative L_2 error)			
function	in each HL	Trained	Testing	Trained (1% Noise)	Testing (1% Noise)	Trained (5% Noise)	Testing (5% Noise)
tanh	[5, 5, 5]	9.2021e−07	1.4912e−06	0.00018143	0.00025223	0.00086409	0.0013559
tanh	[10, 10, 10]	1.0025e−06	1.8416e−06	0.00017612	0.00026251	0.00088679	0.0013736
tanh	[20, 20, 20]	2.0645e−06	1.8425e−06	0.00017262	0.00025973	0.00091399	0.0014292
tanh	[5, 5, 5, 5]	5.3412e−07	8.1092e−07	0.00016468	0.0002604	0.00089185	0.0013972
tanh	[10, 10, 10, 10]	7.3515e−07	1.2747e−06	0.00017616	0.00025679	0.00087464	0.0012712
tanh	[20, 20, 20, 20]	9.1012e−07	2.0379e−06	0.00018352	0.00029509	0.00084639	0.0013802
sigmoid	[5, 5, 5]	4.0744e−07	7.7193e−07	0.00017374	0.00025279	0.00087157	0.0013996
sigmoid	[10, 10, 10]	9.6703e−07	2.0109e−06	0.00017451	0.00027066	0.00083334	0.0015296
sigmoid	[20, 20, 20]	2.4697e−06	5.8662e−06	0.00017631	0.00026908	0.00093604	0.0012481
sigmoid	[5, 5, 5, 5]	5.8084e−07	9.4758e−07	0.00017222	0.00025243	0.00085568	0.0013575
sigmoid	[10, 10, 10, 10]	3.8072e−06	1.4974e−06	0.00016827	0.00026621	0.00091027	0.0014134
sigmoid	[20, 20, 20, 20]	1.978e−05	4.1206e−05	0.00018113	0.00026593	0.00085856	0.0012924

algorithm within an artificial neural network framework, which strengthened the reliability of our results through rigorous statistical analysis. This combined analytical and neural network enabled a thorough exploration of the dynamics of the nonlocal CCD system, bridging theoretical insights with empirical validation.

Future work could expand the analysis of the generalized CD system to more complex configurations of current-fed strings in external magnetic fields, incorporating nonlocal effects. This includes examining how variations in magnetic field strength, current, boundary conditions, and external perturbations influence wave behavior, stability, and nonlinear interactions. We also aim to investigate the development of chaotic dynamics and turbulence under specific conditions, and assess the impact of material properties and temperature variations to enhance the model's applicability to real-world scenarios. On the computational side, we plan to develop unsupervised learning strategies based on PINNs, where the network weights will be optimized using bio-inspired algorithms such as particle swarm optimization (PSO) and genetic algorithms (GA). In parallel, for the LM-ANN framework, we intend to incorporate the regularization techniques to enhance generalization and reduce overfitting in the training process.

Table 6
Solution $\rho^{[2]}$ in (3.6): Model performance with clean and noisy data for $t = 0.5$.

Activation function	No of nodes in each HL	Clean data (Relative L_2 error)		Noise data (Relative L_2 error)			
		Trained	Testing	Trained (1% Noise)	Testing (1% Noise)	Trained (5% Noise)	Testing (5% Noise)
tanh	[5, 5, 5]	0.00024984	0.00030687	0.0002426	0.00043529	0.00073001	0.0011219
tanh	[10, 10, 10]	0.00061781	0.00074252	0.00020918	0.00034875	0.00068497	0.0011235
tanh	[20, 20, 20]	5.4358e−06	1.2935e−05	0.00014342	0.0002293	0.0007006	0.0010899
tanh	[5, 5, 5, 5]	0.00017888	0.0007381	0.00016468	0.00027522	0.00071169	0.0010612
tanh	[10, 10, 10, 10]	4.8607e−06	7.7803e−06	0.00013857	0.00020345	0.00066194	0.0011345
tanh	[20, 20, 20, 20]	3.1935e−06	6.0108e−05	0.000136382	0.00029509	0.00068296	0.0010518
sigmoid	[5, 5, 5]	6.6285e−05	0.00019839	0.00014917	0.00028424	0.00066415	0.0010335
sigmoid	[10, 10, 10]	2.4066e−05	9.4161e−05	0.00015303	0.00021903	0.0006821	0.0010697
sigmoid	[20, 20, 20]	0.00015388	0.0011209	0.00013789	0.00029984	0.00066926	0.00098081
sigmoid	[5, 5, 5, 5]	0.00021223	0.00037656	0.00024742	0.00042597	0.0045414	0.007016
sigmoid	[10, 10, 10, 10]	5.4107e−06	7.8939e−05	0.00013876	0.00021922	0.00071248	0.00118
sigmoid	[20, 20, 20, 20]	1.0084e−05	1.0084e−05	0.00013891	0.00022801	0.00066258	0.0010335

CRediT authorship contribution statement

Aamir Farooq: Writing – original draft, Software, Conceptualization, Validation, Formal analysis. **H.W.A. Riaz:** Writing – review & editing, Visualization, Methodology, Writing – original draft, Software, Conceptualization. **Wen Xiu Ma:** Writing – review & editing, Project administration, Supervision, Conceptualization.

Declaration of competing interest

The authors declare that they have no known competing financial interests or personal relationships that could have appeared to influence the work reported in this paper.

Acknowledgments

H.W.A.R. acknowledges the postdoctoral fellowship supported by Zhejiang Normal University, China, under Grants No. ZC304023926. Wen Xiu Ma acknowledges support from the Ministry of Science and Technology of China (G2021016032L and G2023016011L), the National Natural Science Foundation of China (NSFC) under grants 12271488 and 11975145.

Data availability

The data supporting this study's findings are available in the article.

References

[1] Hiroshi Kakuhata, Kimiaki Konno, Loop soliton solutions of string interacting with external field, J. Phys. Soc. Japan 68 (3) (1999) 757–762.
[2] Hiroshi Kakuhata, Kimiaki Konno, Lagrangian, Hamiltonian and conserved quantities for coupled integrable, dispersionless equations, J. Phys. Soc. Japan 65 (1) (1996) 1–2.
[3] H. Kakuhata, K. Konno, A generalization of coupled integrable, dispersionless system, J. Phys. Soc. Japan 65 (2) (1996) 340–341.
[4] H. Kakuhata, K. Konno, Canonical formulation of a generalized coupled dispersionless system, J. Phys. A: Math. Gen. 30 (12) (1997) L401.
[5] K. Takasaki, T. Takebe, Integrable hierarchies and dispersionless limit, Rev. Math. Phys. 7 (05) (1995) 743–808.
[6] Liming Ling, Bao-Feng Feng, Zuonong Zhu, Multi-soliton, multi-breather and higher order rogue wave solutions to the complex short pulse equation, Phys. D: Nonlinear Phenom. 327 (2016) 13–29.
[7] H. Riaz, A. Wajahat, M. Hassan, Dressing method for the multicomponent short-pulse equation, Theoret. and Math. Phys. 199 (2019) 709–718.
[8] Wei-Guo Zhang, Meng-Yu Wang, Caiqin Song, Soliton solutions of the semi-discrete complex coupled dispersionless integrable system, Appl. Math. Lett. 113 (2021) 106859.
[9] Sen-Yue Lou, Guo-Fu Yu, A generalization of the coupled integrable dispersionless equations, Math. Methods Appl. Sci. 39 (14) (2016) 4025–4034.
[10] H. Riaz, Wajahat A., Mahmood ul Hassan, Multi-component semi-discrete coupled dispersionless integrable system, its lax pair and Darboux transformation, Commun. Nonlinear Sci. Numer. Simul. 61 (2018) 71–83.
[11] Michał Wróbel, Katarzyna Nieszporek, Janusz T Starczewski, Andrzej Cader, A fuzzy measure for recognition of handwritten letter strokes, in: Artificial Intelligence and Soft Computing: 17th International Conference, ICAISC 2018, Zakopane, Poland, June 3-7, 2018, Proceedings, Part I 17, Springer, 2018, pp. 761–770.
[12] Robert K. Nowicki, Janusz T. Starczewski, A new method for classification of imprecise data using fuzzy rough fuzzification, Inform. Sci. 414 (2017) 33–52.
[13] Arthur Barbosa, Joao Pedro Sena, Najib Kacem, Noureddine Bouhaddi, An artificial intelligence approach to design periodic nonlinear oscillator chains under external excitation with stable damped solitons, Mech. Syst. Signal Process. 205 (2023) 110879.
[14] Ismail Onder, Abdulkadir Sahiner, Aydin Secer, Mustafa Bayram, Soliton solutions of some ocean waves supported by physics informed neural network method, in: Artificial Intelligence and Applications, Vol. 2, 2024, pp. 299–308.
[15] Yang-Hui He, AI-driven research in pure mathematics and theoretical physics, Nat. Rev. Phys. 6 (9) (2024) 546–553.
[16] Terrence J. Sejnowski, The Deep Learning Revolution, MIT Press, 2018.

[17] Daron Acemoglu, David Autor, Jonathon Hazell, Pascual Restrepo, Artificial intelligence and jobs: Evidence from online vacancies, J. Labor Econ. 40 (S1) (2022) S293–S340.
[18] Gerald C. Hsu, Using math-physical medicine and artificial intelligence technology to manage lifestyle and control metabolic conditions of T2D, Int. J. Diabetes Complicat. 2 (3) (2018) 1–7.
[19] Paul Werbos, Beyond Regression: New Tools for Prediction and Analysis in the Behavioral Sciences (Ph.D. thesis), Committee on Applied Mathematics, Harvard University, Cambridge, MA, 1974.
[20] Scott E. Fahlman, et al., An Empirical Study of Learning Speed in Back-Propagation Networks, Carnegie Mellon University, Computer Science Department Pittsburgh, PA, USA, 1988.
[21] Martin T. Hagan, Mohammad B. Menhaj, Training feedforward networks with the marquardt algorithm, IEEE Trans. Neural Netw. 5 (6) (1994) 989–993.
[22] Maziar Raissi, Paris Perdikaris, George E. Karniadakis, Physics-informed neural networks: A deep learning framework for solving forward and inverse problems involving nonlinear partial differential equations, J. Comput. Phys. 378 (2019) 686–707.
[23] Gang-Zhou Wu, Yin Fang, Yue-Yue Wang, Guo-Cheng Wu, Chao-Qing Dai, Predicting the dynamic process and model parameters of the vector optical solitons in birefringent fibers via the modified PINN, Chaos Solitons Fractals 152 (2021) 111393.
[24] Run-Fa Zhang, Sudao Bilige, Bilinear neural network method to obtain the exact analytical solutions of nonlinear partial differential equations and its application to p-gBKP equation, Nonlinear Dynam. 95 (2019) 3041–3048.
[25] Run-Fa Zhang, Sudao Bilige, Jian-Guo Liu, Mingchu Li, Bright-dark solitons and interaction phenomenon for p-gBKP equation by using bilinear neural network method, Phys. Scr. 96 (2) (2020) 025224.
[26] Runfa Zhang, Sudao Bilige, Temuer Chaolu, Fractal solitons, arbitrary function solutions, exact periodic wave and breathers for a nonlinear partial differential equation by using bilinear neural network method, J. Syst. Sci. Complex. 34 (1) (2021) 122–139.
[27] Chun-Yan Qin, Run-Fa Zhang, Yao-Hong Li, Various exact solutions of the (4+ 1)-dimensional Boiti–Leon–Manna–Pempinelli-like equation by using bilinear neural network method, Chaos Solitons Fractals 187 (2024) 115438.
[28] Run-Fa Zhang, Ming-Chu Li, Amina Cherraf, Shashank Reddy Vadyala, The interference wave and the bright and dark soliton for two integro-differential equation by using BNNM, Nonlinear Dynam. 111 (9) (2023) 8637–8646.
[29] Run-Fa Zhang, Ming-Chu Li, Bilinear residual network method for solving the exactly explicit solutions of nonlinear evolution equations, Nonlinear Dynam. 108 (1) (2022) 521–531.
[30] Ilya Sutskever, James Martens, George Dahl, Geoffrey Hinton, On the importance of initialization and momentum in deep learning, in: International Conference on Machine Learning, PMLR, 2013, pp. 1139–1147.
[31] Hiroshige Dan, Nobuo Yamashita, Masao Fukushima, Convergence properties of the inexact Levenberg–Marquardt method under local error bound conditions, Optim. Methods Softw. 17 (4) (2002) 605–626.
[32] Jinyan Fan, Jianyu Pan, Convergence properties of a self-adaptive Levenberg–Marquardt algorithm under local error bound condition, Comput. Optim. Appl. 34 (1) (2006) 47–62.
[33] Andreas Fischer, Alexey F. Izmailov, Mikhail V. Solodov, The Levenberg–Marquardt method: an overview of modern convergence theories and more, Comput. Optim. Appl. (2024) 1–35.
[34] A. Waheed, M. Awais, M.A.Z. Raja, M.Y. Malik, A.S. Alqahtani, Peakon and solitary wave solutions of the LAX equation: Neuro computing procedure, Int. Commun. Heat Mass Transfer 152 (2024) 107321.
[35] H.W.A. Riaz, Aamir Farooq, A (2+ 1) modified KdV equation with time-dependent coefficients: exploring soliton solution via darboux transformation and artificial neural network approach, Nonlinear Dynam. (2024) 1–17.
[36] Mark J Ablowitz, Bao-Feng Feng, Xu-Dan Luo, Ziad H Musslimani, Reverse space-time nonlocal sine-Gordon/sinh-Gordon equations with nonzero boundary conditions, Stud. Appl. Math. 141 (3) (2018) 267–307.
[37] Jia-Liang Ji, Jun Yang, Zuo-Nong Zhu, Multi-soliton solutions for a nonlocal complex coupled dispersionless equation, Commun. Nonlinear Sci. Numer. Simul. 82 (2020) 105028.
[38] M.J. Ablowitz, P.A. Clarkson, Solitons, Nonlinear Evolution Equations and Inverse Scattering, Vol. 149, Cambridge University Press, 1991.
[39] A. Constantin, R.I. Ivanov, J. Lenells, Inverse scattering transform for the Degasperis–Procesi equation, Nonlinearity 23 (10) (2010) 2559.
[40] A.K. Pogrebkov, Hirota difference equation: Inverse scattering transform, Darboux transformation, and solitons, Theoret. and Math. Phys. 181 (3) (2014) 1585–1598.
[41] S. Liu, B. Tian, M. Wang, Painlevé analysis, bilinear form, Bäcklund transformation, solitons, periodic waves and asymptotic properties for a generalized Calogero–Bogoyavlenskii–Konopelchenko–Schiff system in a fluid or plasma, Eur. Phys. J. Plus 136 (9) (2021) 1–18.
[42] Y. Xia, R. Yao, X. Xin, Y. Li, Nonlocal symmetry, Painlevé integrable and interaction solutions for CKdV equations, Symmetry 13 (7) (2021) 1268.
[43] K. Konno, M. Wadati, Simple derivation of Bäcklund transformation from Riccati form of inverse method, Progr. Theoret. Phys. 53 (6) (1975) 1652–1656.
[44] Yu-Hang Yin, Xing Lü, Wen-Xiu Ma, Bäcklund transformation, exact solutions and diverse interaction phenomena to a (3+ 1)-dimensional nonlinear evolution equation, Nonlinear Dynam. 108 (4) (2022) 4181–4194.
[45] L. Luo, Bäcklund transformation of variable-coefficient Boiti–Leon–Manna–Pempinelli equation, Appl. Math. Lett. 94 (2019) 94–98.
[46] Xin-Yi Gao, Yong-Jiang Guo, Wen-Rui Shan, Shallow water in an open sea or a wide channel: Auto-and non-auto-Bäcklund transformations with solitons for a generalized (2+ 1)-dimensional dispersive long-wave system, Chaos Solitons Fractals 138 (2020) 109950.
[47] ED Belokolos, AI Bobenko, VZ Enolskii, AR Its, VB Matveev, Algebro-Geometric Approach to Nonlinear Integrable Equations, Vol. 550, Springer-Verlag, 1994.
[48] Zheng Li, Muwei Liu, Yan Jiang, Wenjun Liu, Step-like soliton solutions and dynamic behavior of solitons in the inhomogeneous fiber optics, Nonlinear Dynam. 112 (10) (2024) 8495–8505.
[49] Haotian Wang, Hujiang Yang, Xiankui Meng, Ye Tian, Wenjun Liu, Dynamics of controllable matter-wave solitons and soliton molecules for a rabi-coupled Gross–Pitaevskii equation with temporally and spatially modulated coefficients, SIAM J. Appl. Dyn. Syst. 23 (1) (2024) 748–778.
[50] Haotian Wang, Hujiang Yang, Ye Tian, Wenjun Liu, Controllable nonautonomous localized waves and dynamics for a quasi-1D Gross–Pitaevskii equation in Bose–Einstein condensations with attractive interaction, Chaos: An Interdiscip. J. Nonlinear Sci. 34 (5) (2024) 053125.
[51] V.B. Matveev, M.A. Salle, Darboux Transformations and Solitons, Springer Berlin Heidelberg, 1991.
[52] Li-Yuan Ma, Yan-Li Zhang, Li Tang, Shou-Feng Shen, New rational and breather solutions of a higher-order integrable nonlinear Schrödinger equation, Appl. Math. Lett. 122 (2021) 107539.
[53] Haotian Wang, Qin Zhou, Hujiang Yang, Xiankui Meng, Ye Tian, Wenjun Liu, Modulation instability and localized wave excitations for a higher-order modified self-steepening nonlinear Schrödinger equation in nonlinear optics, Proc. R. Soc. A 479 (2279) (2023) 20230601.
[54] Roman O. Popovych, Alexander L. Sakhnovich, GBDT version of the Darboux transformation for the matrix coupled dispersionless equations (local and non-local cases), J. Integr. Syst. 5 (1) (2020) xyaa004.
[55] H. Riaz, Wajahat A., Darboux transformation and exact multisolitons for a matrix coupled dispersionless system, Commun. Theor. Phys. (Beijing) 72 (7) (2020) 075001.
[56] Wang Tang, Guo-Fu Yu, Shou-Feng Shen, Rogue periodic waves of the short pulse equation and the coupled integrable dispersionless equation, Wave Motion 124 (2024) 103234.
[57] Hong-Qian Sun, Zuo-Nong Zhu, Darboux transformation and soliton solutions of the spatial discrete coupled complex short pulse equation, Phys. D: Nonlinear Phenom. 436 (2022) 133312.

[58] Kemal Eren, Soley Ersoy, Complex coupled dispersionless equations in Minkowski 3-space, Complex Var. Elliptic Equ. 68 (11) (2023) 1984–1999.
[59] Hayrettin Okut, Daniel Gianola, Guilherme JM Rosa, Kent A Weigel, Prediction of body mass index in mice using dense molecular markers and a regularized neural network, Genet. Res. 93 (3) (2011) 189–201.
[60] Inmaculada Alados, José Antonio Mellado, Francisca Ramos, Lucas Alados-Arboledas, Estimating UV erythemal irradiance by means of neural networks¶, Photochem. Photobiol. 80 (2) (2004) 351–358.
[61] David J.C. MacKay, Information Theory, Inference and Learning Algorithms, Cambridge University Press, 2003.